Journal of The Electrochemical Society, **153** (10) B434-B445 (2006)
0013-4651/2006/153(10)/B434/12/$20.00 © The Electrochemical Society

Electrochemical and Structural Characterization of Heat-Treated Cr_3C_2–NiCr Coatings

P. H. Suegama,[a] N. Espallargas,[b] J. M. Guilemany,[b] J. Fernández,[b] and A. V. Benedetti[a,*,z]

[a]*Departamento de Físico-Química, Instituto de Química da Universidade Estadual Paulista, 14801-970 Araraquara, SP, Brazil*
[b]*CPT Thermal Spray Centre, Materials Engineering, Departament de Ciència dels Materials i Enginyeria Metallúrgica, Universitat de Barcelona, E-08028 Barcelona, Spain*

The influence of heat-treatments on the electrochemical behavior of thermal spray Cr_3C_2–NiCr coatings prepared by high velocity oxygen fuel (HVOF) was studied in NaCl solution, at 25°C, using open-circuit potential (E_{OC}) and electrochemical impedance spectroscopy (EIS) measurements. Coating characterization were performed before and after the heat-treatments and electrochemical tests by scanning electron microscopy, X-ray diffraction, and Auger electron spectroscopy. In addition to the changes in the original powder composition occurring during HVOF process, heat-treatment performed at 450°C caused no significant changes in electrochemical response compared with untreated sample, and at 760°C the main difference was the formation of a thin and defective layer of Cr_2O_3 at the coating surface, which increased the total impedance at the first day of immersion. Higher influence on the electrochemical was noted for samples treated at 880°C, which also showed higher E_{OC} and total impedance, and lower corrosion current. This behavior was interpreted considering the formation of a chromium oxide layer on the coating surface, dissolution and decomposition of smaller carbide particles and their surface enrichment with Cr due to C diffusion and dissolution into the matrix, and possible Ni, Cr, and Fe diffusion to coating/substrate interface.
© 2006 The Electrochemical Society. [DOI: 10.1149/1.2229288] All rights reserved.

Manuscript submitted January 23, 2006; revised manuscript received May 8, 2006. Available electronically August 18, 2006.

Thermally sprayed Cr_3C_2–NiCr coatings are widely used in aircraft manufacturing, automotive industry, paper manufacturing machinery, and other engineering applications due to their good tribological and corrosion-oxidation properties in aggressive environments.[1,2] These facts place them as an alternative to hard chromium plating in applications where both wear and corrosion resistance are required.[3,4]

With high velocity oxygen fuel (HVOF) processes, low porosity metallic and cermets coatings can be obtained at deposition rates faster than those for electroplating, and with good oxidation resistance and adherence properties.[5,6] However, these coatings only present corrosion resistance in aqueous salt solutions if all spraying parameters, powder morphology, and composition are optimized.

Cr_3C_2–NiCr coatings have sprayed using a CDS gun with optimized propylene/oxygen ratio, spraying distance, gun displacement, and number of torch passes.[7-11] Coatings obtained were studied in sulfuric acid and neutral chloride solutions and during the first 12 h of immersion they showed a lower electrolyte penetration velocity delaying substrate corrosion. However, Cr_3C_2–NiCr coatings sprayed with a HVOF DJ 2700 gun[12] using a Diamalloy 3007 powder showed higher corrosion resistance in 3.4% NaCl solution even immersed up to 100 h of test, compared with those obtained with the CDS gun. Moreover, it was shown that the combination of optimized spraying parameters and heat-treatments (made with the gun flame) improved their corrosion resistance.[8,13] For instance, Cr_3C_2–NiCr coatings showed no appreciable electrolyte attack at the coating/substrate interface after 24 h of immersion in sulfuric acid solution. Despite these results, these coatings showed low corrosion resistance.

Studies involving combined erosion and corrosion tests were also performed for cermets at different conditions and electrolyte solutions.[9,14,15] They showed some synergism between corrosion and wear, increasing the degradation of the coating due to a faster corrosion process caused by a continuous material removal. Cermets coatings prepared using conventional size particle powders underwent higher mass loss than those prepared with nanoparticle powders. It seems that the main mechanism of coating degradation is the electrolyte penetration through the defects, mainly at the brittle particles/metallic matrix interface. Even when the metallic matrix could offer a good corrosion resistance by passivation, the defects allow the aggressive ions to attack the matrix avoiding the formation of a passive film.

Our experience showed that electrochemical response of cermets coatings are extremely dependent on the history of coating preparation and post-treatment due to defects and new phases introduced during spray processes. For instance, during the particles flight, the composition of the initial phases of the powder changes: oxidation and decomposition of particles take place resulting in the formation of a well-distributed Cr_2O_3 phase,[16] decomposition of the Cr_3C_2 phase into Cr_7C_3 and $Cr_{23}C_6$ occurs, and dissolution of the carbide into the alloy matrix can occur.[17-19] He et al.[17] showed that Cr_2O_3 is directly formed from the reaction of chromium carbide with oxygen. It was also shown that during the formation and buildup of the nanostructured and conventional Cr_3C_2–NiCr coatings an amorphous phase (supersaturated matrix) was formed due to the rapid cooling of the coating.[17-19] Matthews et al.[19] sprayed these coatings by two different high velocity spraying techniques (HVOF and HVAF), and then heat-treated at different temperatures and times. The authors[19] found that the carbide dissolution during spraying led to supersaturation of chromium and carbon inside the matrix and during heat-treatment, the chromium and carbon content in the matrix were diminished. They also found that HVOF coatings showed higher carbide decomposition than the ones obtained with HVAF. These results indicate that post-treatments are also important to define the final properties of the cermets coatings.

Cr_3C_2–NiCr coatings are widely used in aeronautic applications due to its high wear resistance at temperatures up to 850°C.[20] But, wear properties at room temperature of a heat-treated Cr_3C_2–NiCr coating is not improved due to the Cr_2O_3 formation.[1] Then, the temperatures used in this work were chosen taking into account three facts: (*i*) 450°C is the temperature where crystallization begins, (*ii*) at 760°C starts the Cr_xC_y transformation, the carbide precipitation in the supersaturated matrix and the chromium oxide formation, and (*iii*) 880°C is the maximum working temperature where the oxygen diffusion continues giving as a result the formation of a passive layer, as well as a carbide growth and coalescence.

Therefore, the aim of this work was to study the influence of heat-treatments on the electrochemical behavior of the coating in salt solution and correlate the electrochemical response with the microstructure evolution. Thus, the electrochemical behavior in NaCl 3.4% solution of untreated and heat-treated Cr_3C_2–NiCr coatings was compared.

* Electrochemical Society Active Member.
z E-mail: benedeti@iq.unesp.br

Downloaded on 2014-01-15 to IP 200.145.3.46 address. Redistribution subject to ECS license or copyright; see ecsdl.org/site/terms_use

Experimental

UNS-G41350 steel was used as substrate. Rectangular (100 × 20 × 5 mm) coupons were degreased with acetone and grid blasted with Al_2O_3 (grade 24) at 5.6 bar, 45° using a blasting distance of 250 mm to get a roughened surface (average roughness, Ra, ~5 μm).

A commercial Amdry 5260 75% Cr_3C_2–25% NiCr (wt %) powder with a size distribution of −45 + 11 μm was sprayed onto the steel substrate. Coatings were obtained using Sulzer Metco (Westbury, NY) Diamond Jet Hybrid DJH 2700 HVOF equipment with oxygen and propylene as a fuel gas.

Cr_3C_2–NiCr coatings (denoted as C20) were obtained with optimized spraying parameters. Heat-treatments (HT) of these samples were done after spraying process at different temperatures (450, 760, and 880°C) in air atmosphere. Samples heated at 450, 760, and 880°C (denoted as 450HT, 760HT, and 880HT, respectively) were treated for 1 h and samples heated at 880°C (denoted as 880HT12 and 880HT24) for 12 and 24 h, respectively. The cooling was carried out inside the furnace in air atmosphere.

The thickness of the coatings was determined by image analysis (Matrox Inspector) using cross-sectional images.

The microstructure of all the coatings was studied by scanning electron microscopy (SEM) JEOL 5310 with energy dispersive spectrometer (EDS) analysis coupled.

Cross-sectional microhardness measurements were performed by means of Vickers indentation with a load of 300 g. Values quoted are an average of 20 indentations for each coating.

The structure of powder and coatings was analyzed using an X-ray diffractometer Siemens D500 (Kα(Cu) = 1.54 Å, 40 kV, 30 mA, step 0.05 s) and field-emission SEM (FE-SEM, Hitachi H-4100FE with 30 keV, current of 10 mA and 1.5 nm resolution) to follow the structural changes produced by the spray process and heat-treatment.

Measurements of Auger electron spectroscopy (AES, Physical Electronics GmbH PHI SAM 670 with Schottky Field Emission Source and Multichannel Detector with 10 keV, current of 10 nA and vacuum level of 2×10^{-8} Torr) were done to identify the composition of oxides formed during the spray process and heat-treatments.

The corrosion resistance of samples was evaluated by means of electrochemical measurements in 80 mL of an aerated and unstirred 3.4% NaCl solution. An $Ag|AgCl|KCl_{saturated}$ electrode connected to the solution through a Luggin capillary was used as a reference electrode and a Pt-network was the auxiliary one. A working electrode of each coated sample was fixed at the bottom of the electrochemical cell, exposing a geometric surface area of 0.74 cm^2 to the solution. Experiments at different regions of the sample were performed to verify if the results are representative and reproducible. These experiments are important considering that cermets coatings have randomly distributed defects. No significant differences in EIS diagrams were found, as early observed.[21,22] In this kind of coating, some comments about real area should be added. The real area, which is almost impossible to know, comprises all part of the coating wetted by the electrolyte, suggesting a continuous increase of the area with the immersion time, as a consequence of the electrolyte penetration. This indicates that the real area is higher than the nominal or apparent one, indicated above, because it only corresponds to the geometric surface area.

The E_{OC} and EIS measurements were made using EG&G Parc-273 and Solartron-SI1255 systems. EIS tests were performed applying 10 mV (rms) to the E_{OC} value, from 5×10^4 to 10^{-2} Hz with 7 points/decade. The E_{OC} was measured until iron oxides appeared on the surface. The E_{OC} measurements were stopped several times to record impedance diagrams, and then the E_{OC} measurement continued. All these tests were conducted at 25°C.

Polarization curves were also recorded for all samples in a potential range from −100 to + 350 mV vs E_{OC} at 0.166 mV s^{-1}, after 24 h of immersion. These curves were registered in two stages:

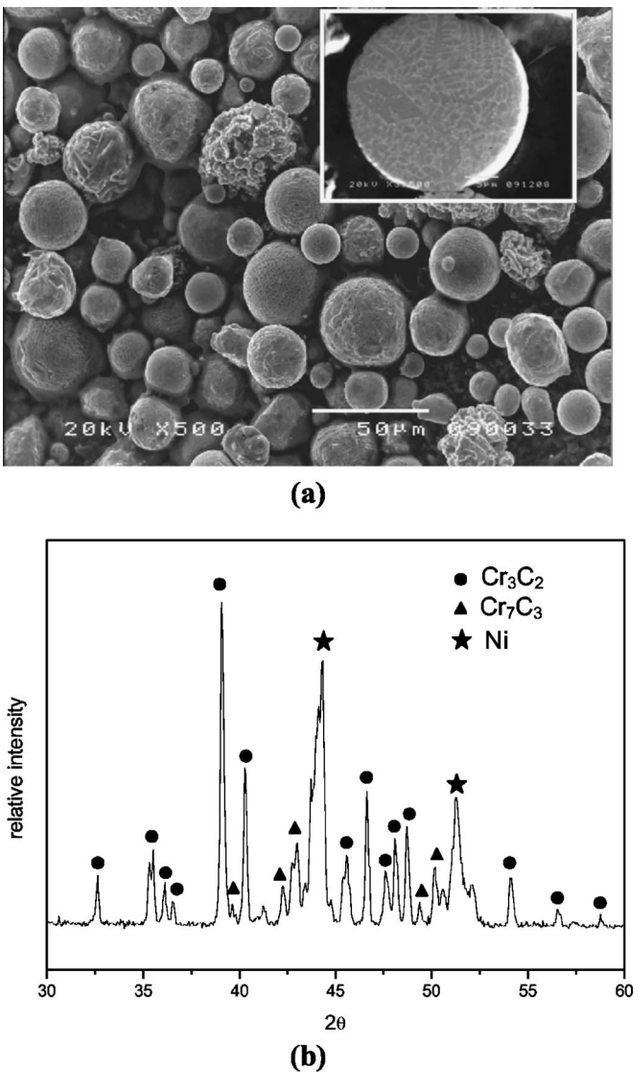

Figure 1. Cr_3C_2–NiCr powder. (a) SEM rough surface (inset: cross section) images and (b) XRD spectrum.

first, starting from E_{OC} and sweeping the potential to the cathodic direction up to −100 mV vs E_{OC} and, second, after reaching the corrosion potential, the anodic curve from the E_{OC} value up to +350 mV vs E_{OC} was recorded. The two curves were merged to give the corresponding total polarization curve.

Results and Discussion

It is well known that the electrochemical response of cermets coatings depends on their structure, which can be modified by post-treatment by heating. We decided to discuss the structural characterization before, in order to facilitate the interpretation of electrochemical results.

Structural characterization.— Cr3C2–NiCr powder.— A commercial Cr_3C_2–NiCr powder with a particle size of −45 +11 μm manufactured by agglomeration and densification was used (Fig. 1a).

The XRD study showed the high crystallinity degree of the powder with the following phases: Cr_3C_2, Cr_7C_3 and NiCr matrix (Fig. 1b).

Coatings.— The structural characterization of the coatings revealed well-bonded layers (no separation between layers was observed). Figure 2a-f shows the SEM images of (a) C20, (b) 450HT, (c)

Downloaded on 2014-01-15 to IP 200.145.3.46 address. Redistribution subject to ECS license or copyright; see ecsdl.org/site/terms_use

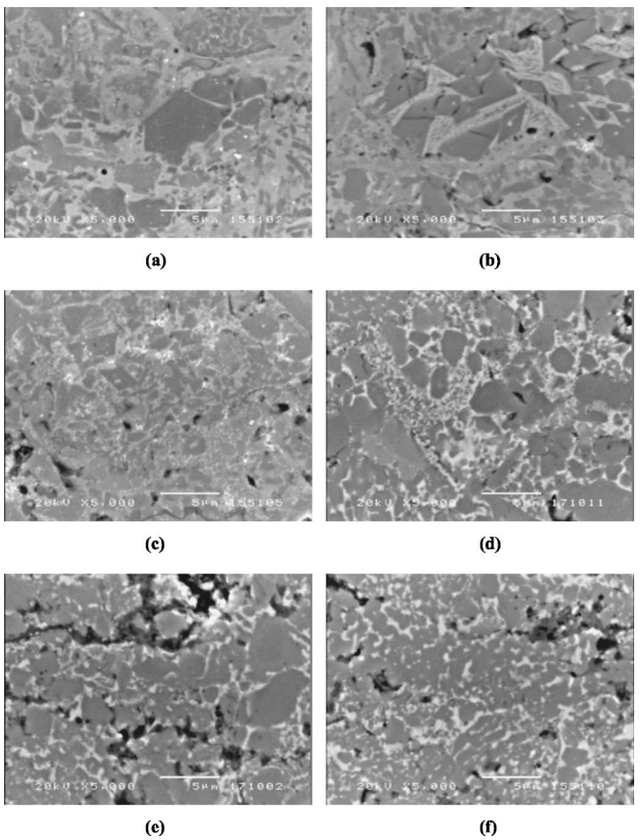

Figure 2. SEM cross-sectional images of (a) C20 sample, (b) 450HT, (c) 760HT, (d) 880HT, (e) 880HT12, and (f) 880HT24.

760HT, (d) 880HT, (e) 880HT12, and (f) 880HT24 coatings, respectively. The structural differences between coatings are due to the extensive carbide dissolution, chromium oxides formation and growth taking place during the spraying process and heat-treatment in air atmosphere (Fig. 2). Carbide dissolution into the matrix and matrix supersaturation are clearly seen from XRD analyses (Fig. 3). The XRD results for C20 and 450HT showed the same phases for both samples indicating that this temperature did not significantly modify the phase composition. The smaller particles of chromium carbide phase are dissolved into the matrix (samples C20 and 450HT) as can be seen from the peaks at 2θ between 40 and 45° (the carbide dissolution promotes the matrix amorphization[22]).

Clark et al.[23] found that the oxidation of the Cr_3C_2 is very slow at temperatures lower than 600°C, which is in agreement with the results obtained here. No oxidation of Cr_3C_2 was found during the heat treatment at 450°C. However, the oxygen diffusion that takes places at this temperature can produce a partial dissolution of the Cr_3C_2 ($D^0_{O-NiCr} = 1.2 \times 10^{-3}$ m^2 s^{-1} in the temperature range of 350 to 1000°C). The dissolution mechanism of this Cr_3C_2 may occur by the C diffusion into the metallic matrix because the diffusion coefficient of C in nickel ($D^0_{C-Ni} = 2.5 \times 10^{-4}$ m^2 s^{-1} in the temperature range of 730 to 1020°C) is higher than the Cr one ($D^0_{Cr-Ni} = 6 \times 10^{-5}$ m^2 s^{-1} in the temperature range of 850 to 1200°C). The higher dissolution of C will produce an outer region of the Cr_3C_2 particles rich in Cr and a C supersaturated NiCr matrix due to the higher C solubility. The diffusion of C decreases as the outer layer is being richer in Cr.[24]

The XRD data of sample heated at 760°C shows both the presence of Cr_2O_3 as a new phase, clearly seen in Fig. 4a which shows a dark phase (pointed by arrows) between carbides and an increase of the Cr_xC_y peaks intensity. The same figure shows a large amount

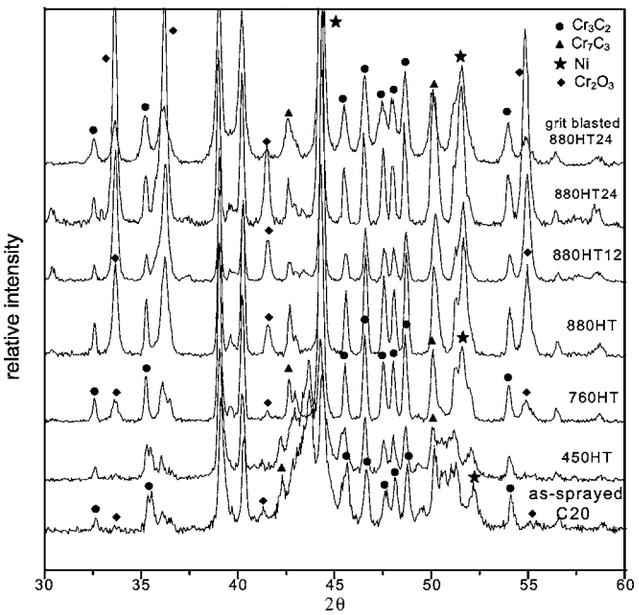

Figure 3. XRD spectra of the samples studied.

of new small chromium carbide particles which are now precipitated from the supersaturated matrix. The oxygen diffusion from the furnace atmosphere into the coating took place at any temperature. The higher the heat-treatment temperature, the greater the oxygen diffusion rate is. As indicated by Clark et al.[25] the oxidation of Cr_3C_2 does not take place at temperatures lower than 650°C. As explained above, the outer Cr rich layer formed as a consequence of the C diffusion is now suitable to reacts with the diffusing O to form the chromium oxide. In this way, the Cr_2O_3 is surrounding the chromium carbide as it can be seen in Fig. 4b.

If this argument is true, the question to be answered now is why there is no Cr_2O_3 on the bigger Cr_3C_2 particles. Young et al.[25] demonstrated that the smaller Cr_3C_2 particles have a higher surface-volume interface, thus giving a higher C diffusion and formation of the Cr rich layer at shorter times. This fact could easily explain why

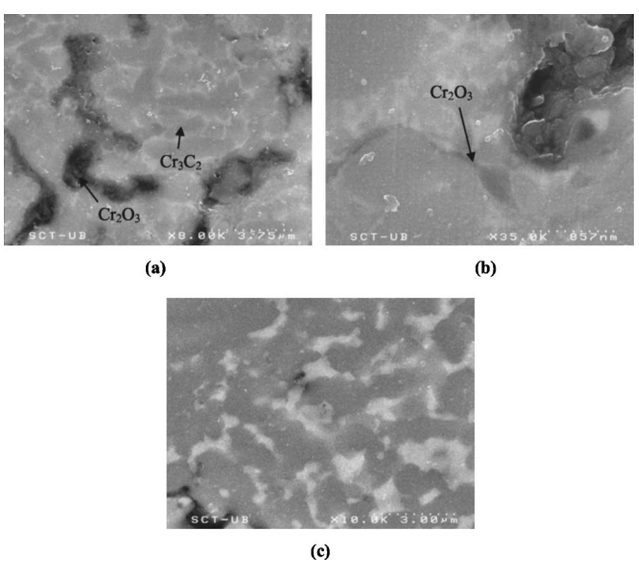

Figure 4. FE-SEMs of (a) 760HT sample, (b) detail of the structure of 760HT, and (c) 880HT24 sample.

Downloaded on 2014-01-15 to IP 200.145.3.46 address. Redistribution subject to ECS license or copyright; see ecsdl.org/site/terms_use

the Cr_2O_3 is found with a laminar morphology around the smaller chromium carbides (Fig. 4b). Also, some amount of Cr_2O_3 oxide can be formed at the coating surface as a result of Cr oxidation by oxygen due to the direct contact of air with the sample surface.

At higher temperatures (880HT) and longer times of heat-treatment (880HT12 and 880HT24), there is a growth and coalescence of the Cr_xC_y precipitates as it can be seen in Fig. 2d-f and 4c. No more Cr_xC_y precipitation seems to take place at 880°C as can be seen from the XRD data (Fig. 3). The oxide amount increases as the heat-treatment time and temperature is increased. After 1 h at 880°C, the oxide content is greater than at 760°C because the oxygen diffusion rate is superior.

Other authors[17,19] also mentioned the formation of a chromium oxide layer on the coating surface during heat-treatment; this phenomenon is clearly seen in Fig. 3, where a XRD spectra of sample 880HT24 was done after removing 50 μm of coating. The intensity of chromium oxide peak significantly diminished after grit blasting.

Only Cr_2O_3 was detected by XRD, but the XRD patterns also show an overlap of Cr–Ni–O phases with the Cr_2O_3 pattern (760HT). AES measurements were done to identify the formed oxides and to study the diffusion processes during the heat-treatment at 760°C (1 h) and 880°C (24 h), with the results shown in Fig. 5. For 760HT sample, the oxides (laminated morphology) are a mixture of Cr–O and Ni–O with different amount of nickel (Fig. 5a and b). Nickel oxides are the result of a kinetic process that takes place during spraying. However, chromium oxides, formed by a thermodynamical process, are more stable than nickel ones (as the Ellingham diagram shows). Thus, the heat-treatment at 760°C (1 h) is not enough to complete the thermodynamic process. The presence of Fe on the coating/substrate interface, clearly seen in Fig. 5c, is mainly due to the diffusion process that takes place during the heat-treatment. Nickel and chromium have a high solubility in iron and, once the coating is heat-treated at high temperature, the diffusion process occurs, leading to dissolution of Ni in the substrate and iron into the coating. This diffusion process increases the coating adherence to the substrate. The adherence of thermal spray coatings is due to a mechanical bonding. Owing to the diffusion process, this mechanical bonding becomes metallurgical leading to a high adherence to the substrate.

However, chromium oxide was the only oxide detected in sample 880HT24 as can be seen from the two spectra in Fig. 5d and e. No nickel oxide was detected in these analyses as it was observed for sample 760HT. The Ni diffusion to the substrate (and iron diffusion to the coating) is greater at 880°C (Fig. 5f) than at 760°C, which is mainly due to the higher temperature and longer times.[26] This diffusion leads to an increase in the corrosion resistance because of the enrichment in Cr on the coating/substrate interface (Fig. 6a and b). This fact and the growth of chromium oxide on the coating surface are the main responsible for the higher impedance measured for this sample, increasing the total impedance as it will be shown ahead.

Thickness and hardness of all coatings are shown in Table I. Heat-treatment has no effect on the thickness of coatings. Samples C20 and 450HT showed the lowest hardness, whereas 760HT and 880HT24 showed an increase of 13 and 21%, respectively. This fact agrees with the formation of new ceramic phases such as chromium oxides and the precipitation of chromium carbides during the heat treatments.

Electrochemical characterization.— Open-circuit measurements.— Figure 7 shows the open-circuit potentials (OCPs) for steel substrate, C20, 450HT, 760HT, and 880HT24 samples during 20 h of immersion. The E_{OC} for the steel substrate decayed sharply from the immersion potential value to around −0.72 V. The steel substrate surface showed pits and great amount of corrosion products, and the solution acquired the typical color of iron(III) ions products after the end of immersion test. For all samples, the E_{OC} decayed abruptly during the first 2 h of immersion to around the following values: −0.57 V (C20 and 450HT), −0.18 V (760HT), and −0.15 V (880HT24). The E_{OC}, after 2 and 20 h of immersion, was almost the same and around −0.59 V for C20 and 450HT samples, which means that the electrolyte rapidly penetrated the coating and reached the substrate, suggesting a more open and/or cracked structure, and also that the heat-treatment at 450°C for 1 h produced no significant changes in structure and phase composition of the C20 sample. The results obtained for C20 and 450HT also suggest that the oxidation of the metallic matrix at the sample surface was not enough to delay the electrolyte penetration and protect the substrate against corrosion. This means that an uniform and/or thick passive layer of chromium and nickel oxides was not produced. For both C20 and 450HT samples iron oxides were observed on top before 20 h of immersion, while for 760HT sample and 880HT series no iron oxides were seen on the top at the same experimental conditions. In a parallel experiment for 760HT, 880HT, 880HT12, and 880HT24 samples the OCPs after 2 h of immersion decayed to −0.31, −0.24, −0.23, and −0.26 V respectively, and no iron oxides were found at the samples surfaces. These results suggest that the heat-treatment, for samples 760HT and 880HT series, makes difficult the electrolyte penetration when compared with C20 and 450HT ones. At 760°C the matrix oxidation was increased, but a little carbide phase decomposition can occur, while at 880°C matrix oxidation and carbide decomposition take place, increasing the passive layer thickness.

In another set of experiments the E_{OC} was recorded for a longer time up to the iron oxides on the surface of 760HT and 880HT series were observed. Impedance data were also acquired for different immersion times during the E_{OC} experiment. This set of experiments allows knowing the evolution of E_{OC} and impedance diagrams with time. Figure 8a-d shows OCP vs time curves for 760HT, 880HT, 880HT12, and 880HT24 samples. E_{OC} was not measured for longer immersion times for C20 and 450HT samples due to the appearance of iron oxides at the top of the samples after 20 h of immersion. The marks EIS1, EIS2 and so on indicate the time and potential were the impedance spectra were performed. For 760HT, a continuous and slower potential decay was observed from the beginning up to 60 h of immersion test, while a faster potential decaying occurred for longer immersion times, reaching an E_{OC} value near −0.5 V after 75 h of test. Iron oxides were observed on the top of the sample after 60 h of immersion, indicating an accelerated corrosion and dissolution of the substrate. This means that the corrosion of the substrate by the electrolyte began at shorter times, and at higher potential compared with the substrate/electrolyte interface (around −0.72 V). Also, it is clear that the passive chromium oxide layer formed on the surface acts as a barrier for electrolyte penetration, delaying the substrate oxidation when compared with samples C20 and 450HT. The passive layer was formed mainly due to the matrix oxidation for 760HT, while for 880HT series both metallic matrix oxidation and carbide phase decomposition and oxidation followed by chromium oxidation contributed to form this layer. The thickness of the passive layer is also expected to increase with time of heat-treatment as observed for 880HT series.

For 880HT series the E_{OC} decreased up to around −0.3 V after few hours of immersion, decreasing very slowly for longer immersion times up to −0.42 V for 880HT (240 h), −0.32 V for 880HT12 (240 h not shown in figure) and −0.25 V for 880HT24 (240 h), and iron oxides were not observed on the top up to 200 h of immersion. The higher temperature and longer heat-treatment time used can be responsible for the higher E_{OC} values because a greater amount of chromium oxide was formed mainly at the surface. Its formation is due to metallic matrix oxidation and carbide phase decomposition, followed by chromium oxidation. It was demonstrated above (Fig. 3) that the amount of chromium oxide at the sample surface increased with the temperature and heat-treatment time. Also, for 880HT24 sample the chromium oxide content decreased after the surface grit blasting, which confirms the formation of the passive layer at the sample surface (Fig. 3). It is also possible that chromium oxide formation and carbides dissolution and re-precipitation into the supersaturated matrix produced some pores closing and matrix

Downloaded on 2014-01-15 to IP 200.145.3.46 address. Redistribution subject to ECS license or copyright; see ecsdl.org/site/terms_use

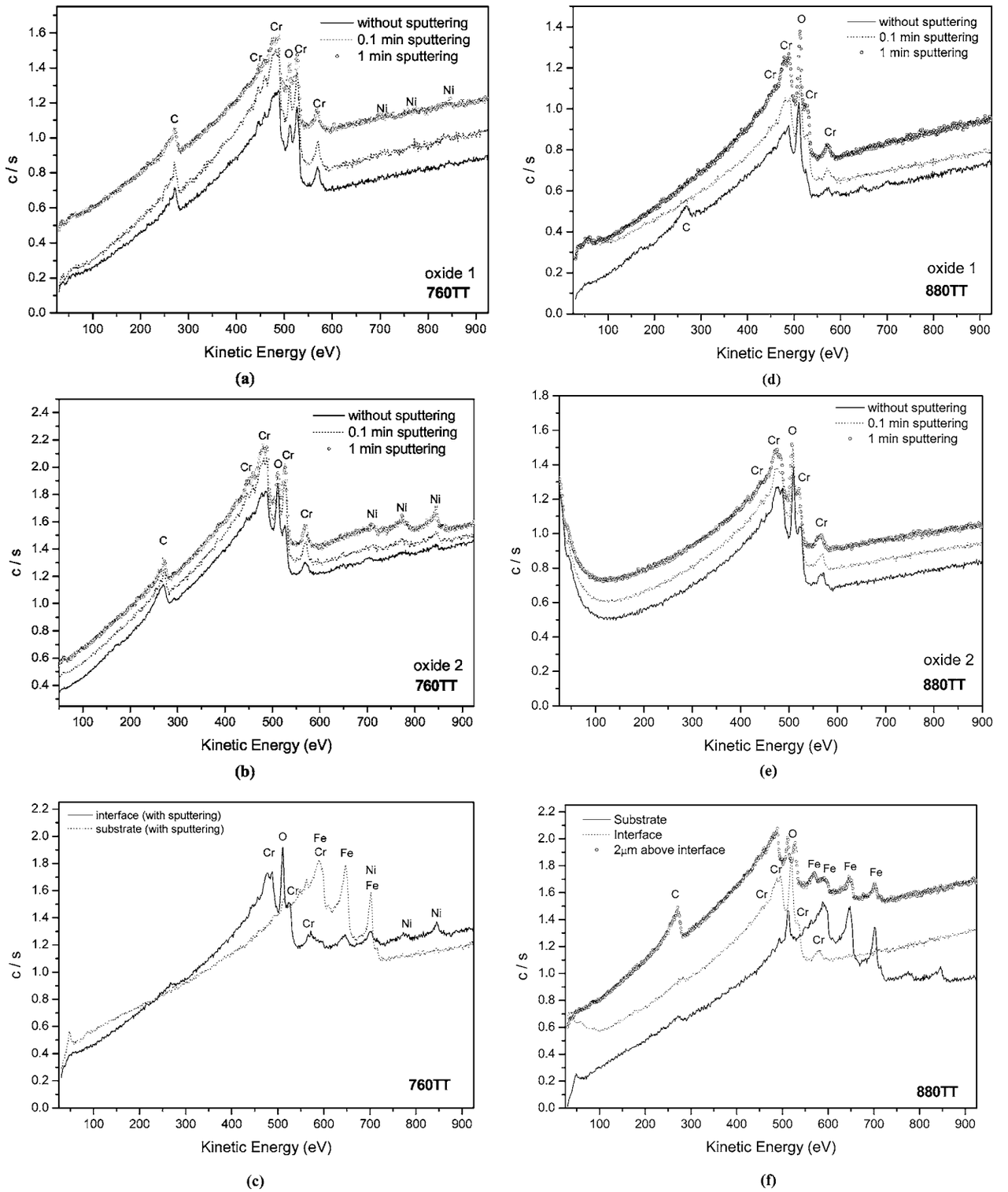

Figure 5. AES spectra of (a) chromium rich oxide in sample 760HT, (b) nickel rich oxide in sample 760HT, (c) coating/substrate interface composition for sample 760TT, (d and e) composition of two different oxides in sample 880HT24, and (f) coating /substrate interface composition for sample 880HT24.

accommodation delaying the electrolyte penetration. We did not have how to prove this statement due to the difficulty of measuring porosity, as by image analysis there is no enough contrast between oxides and pores at the matrix; the mercury intrusion method failed and methods based on volumetric adsorption analysis (using for instance ASAP equipments) are not applied for large pores, besides the coating should be detached from the substrate for the measurement. However, the substrate corrosion resistance probably comes from the chromium oxide layer formed on the sample surface and some Cr-enrichment of the coating/substrate interface. Therefore,

Downloaded on 2014-01-15 to IP 200.145.3.46 address. Redistribution subject to ECS license or copyright; see ecsdl.org/site/terms_use

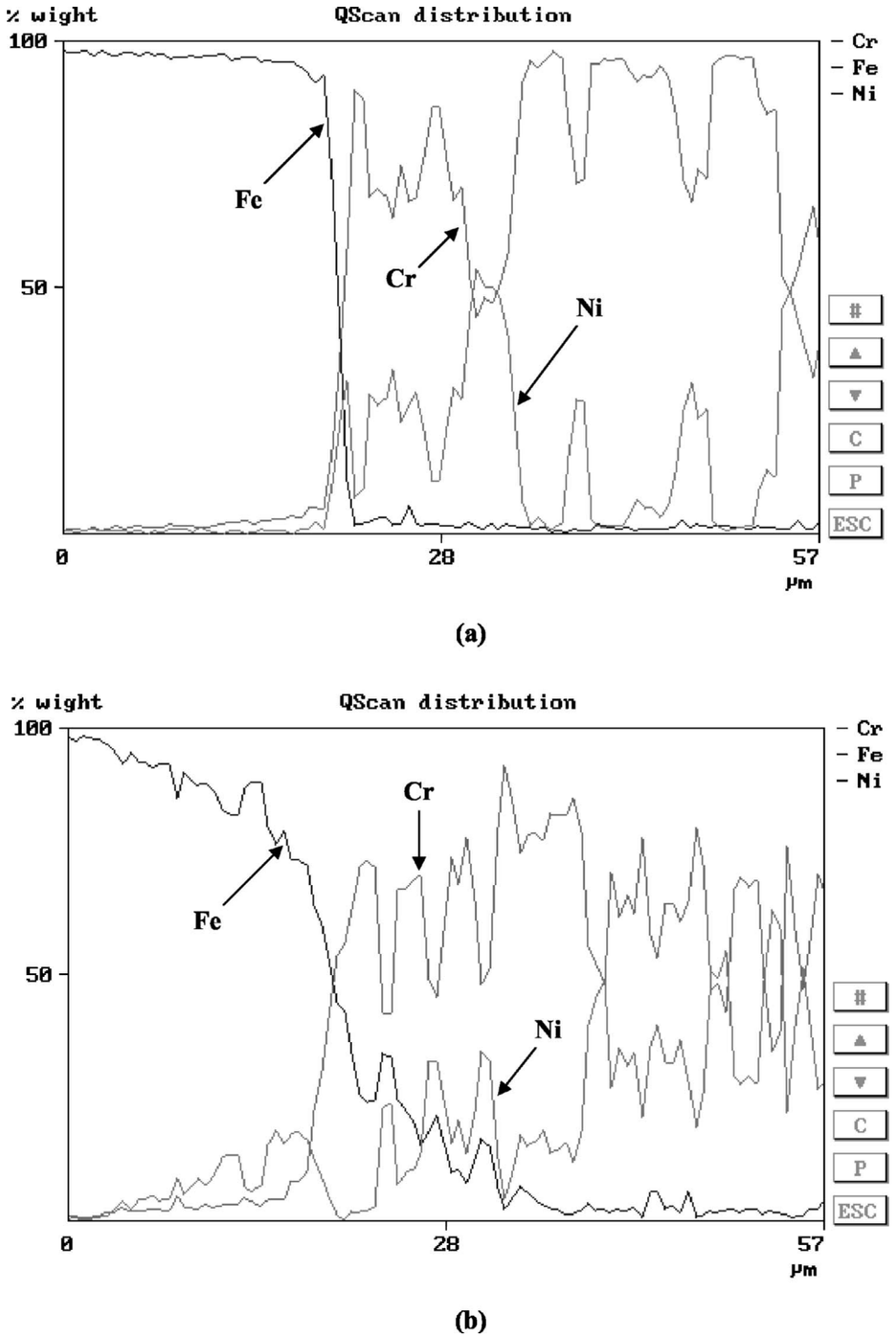

Figure 6. Line-profile of the coating/substrate interface showing the diffusion process during heat-treatment at (a) 760°C for 1 h and (b) 880°C for 24 h.

the higher content of chromium oxides can explain the higher E_{OC} values measured for 880HT series and the differences in EIS diagrams compared to 760HT sample.

EIS measurements.— Impedance experiments for C20 and 450HT samples were carried out after 20 h of immersion. Figure 9 shows Nyquist and Bode plots for C20 and 450HT samples where a very

Table I. Thickness and hardness of coatings tested.

	As-sprayed (C20)	450HT	760HT	880HT	880HT12	880HT24
Thickness (µm)	370 ± 8	350 ± 10	364 ± 8	352 ± 5	370 ± 12	342 ± 11
Hardness ($HVN_{0.3}$)	770 ± 39	748 ± 80	871 ± 30	920 ± 34	960 ± 24	930 ± 60

Downloaded on 2014-01-15 to IP 200.145.3.46 address. Redistribution subject to ECS license or copyright; see ecsdl.org/site/terms_use

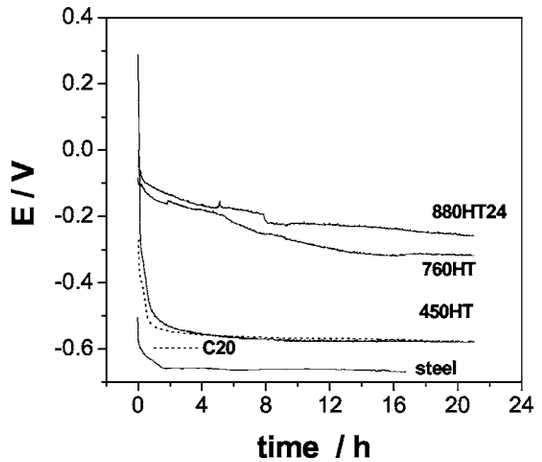

Figure 7. OCP (E_{OC}) vs time curves for steel substrate, and for coated steel samples, obtained in aerated and unstirred 3.4% NaCl solution, at 25°C.

low polarization resistance and at least two time constants were observed. The first one, attributed to the coating, appears at high frequencies, with a maximum around 30 and 100 Hz for C20 and 450HT samples, respectively, with a phase angle around 40°. The second time constant, attributed to the substrate oxidation, appears at around 60 and 100 mHz for C20 and 450HT samples, respectively, with a phase angle around 50 and 40°, respectively. The low total impedance around 1 kΩ for both samples indicates a very poor protection of the substrate and that the electrolyte already reached the substrate producing corrosion. The corrosion is accelerated due to the galvanic pair formed between the nobler coating and steel.

Based on this qualitative analysis and considering the structure of the coating (see characterization section) a scheme representing the surface could be suggested (Fig. 9c). It is supposed that the system can be represented by (a) coating layer (metallic matrix, carbides, metallic oxides, and defects), where a thin and discontinuous chromium oxide-enriched film is probably formed on the coating surface, but it could contribute a little to the impedance response of the coating and was not included separately in the equivalent circuit, and by (b) a coating/substrate interface with some metallic oxides where the main contribution comes from the substrate oxidation. Therefore, the experimental data were simulated using an equivalent electrical circuit (Fig. 9d) with two in series [RCPE] sub-circuits, which are in series with the electrolyte resistance (R_s around 20 Ω at the experimental conditions used). The first [$RCPE_1$] sub-circuit was attributed to the coating response and the second one to the substrate oxidation. The CPE is the constant phase element for the coating or the substrate/solution interface, and substitutes the capacitance, C, for an inhomogeneous surface.[27-29] The CPE is composed by two parameters: Y_0 and n and a value of $n = 1$ corresponds to a smooth surface and/or homogeneous charge distribution on the surface and should be substituted by C. In the present study, at a high frequency range an n around 0.5 was obtained, which is probably related to the porous nature of the

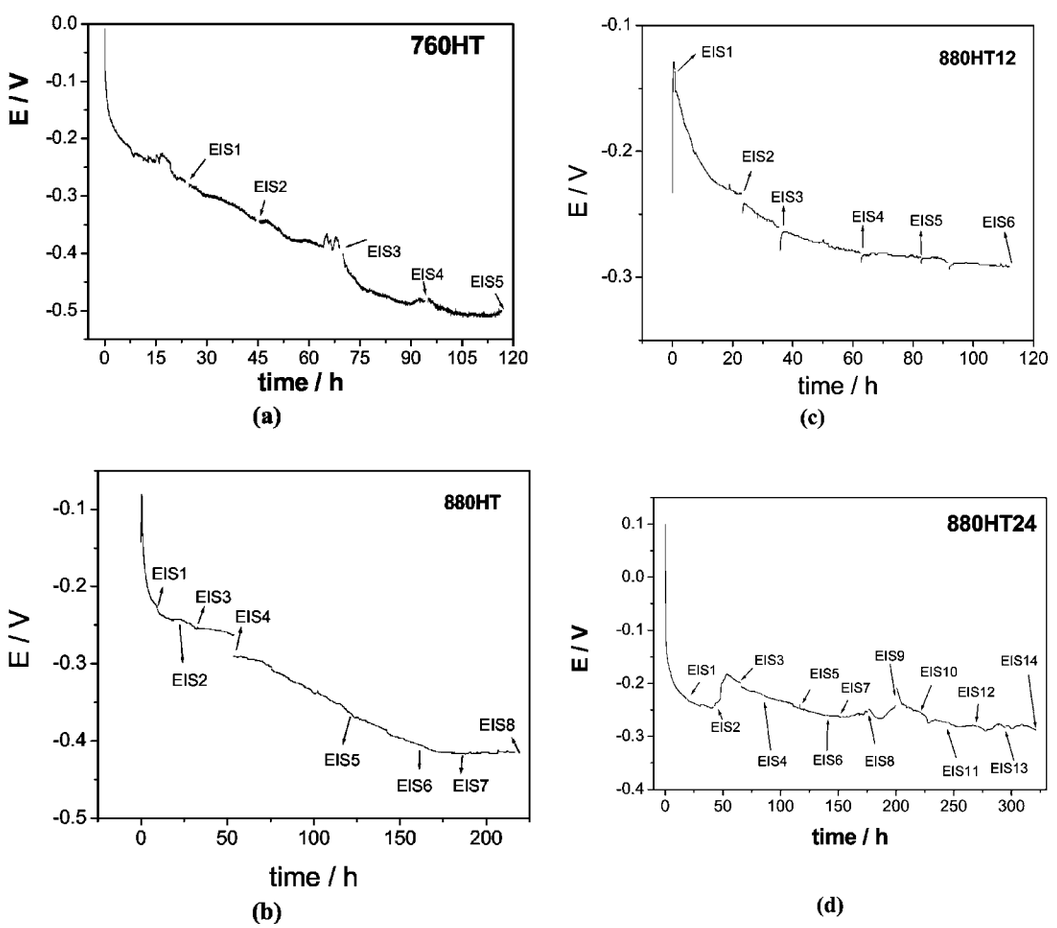

Figure 8. OCP (E_{OC}) vs time curves for (a) 760HT, (b) 880HT, (c) 880HT12, and (d) 880HT24 coatings obtained in aerated and unstirred 3.4% NaCl solution, at 25°C. Geometric surface area of working electrode was 0.74 cm^2.

Downloaded on 2014-01-15 to IP 200.145.3.46 address. Redistribution subject to ECS license or copyright; see ecsdl.org/site/terms_use

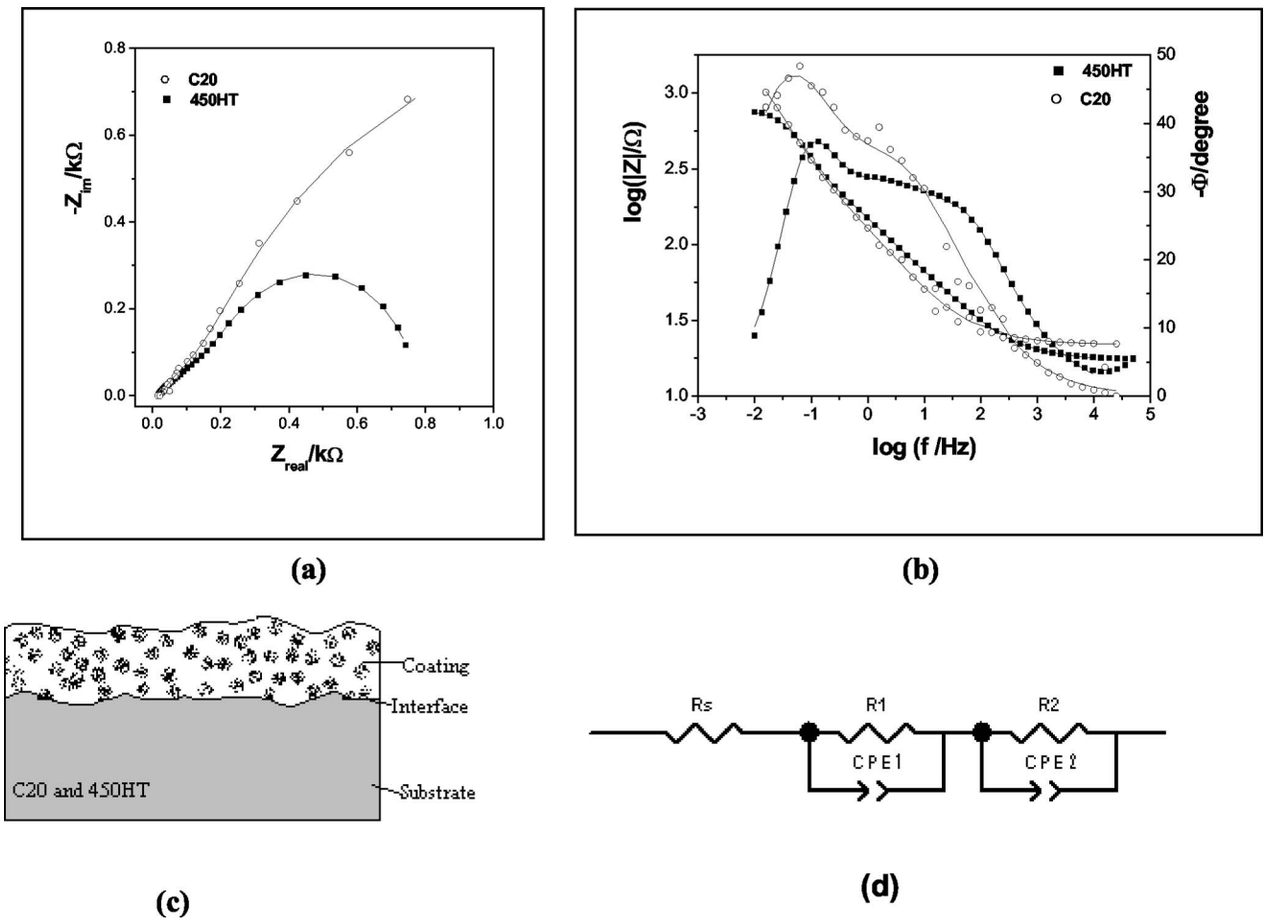

Figure 9. Experimental (symbol) and simulated (solid line): (a) Nyquist, (b) log $|Z|$ and $-\phi$ vs log(f) Bode plots for C20 and 450HT samples in aerated and unstirred 3.4% NaCl solution. (c) Scheme proposed for C20 and 450HT samples, and (d) equivalent electrical circuit used for fitting the experimental data. Geometric surface area of working electrode was 0.74 cm^2.

coating.[30] The $0.5 < n < 1$ values, also observed for C20 and 450HT samples at lower frequency range should be attributed to the substrate surface heterogeneity, roughness, and lack of homogeneity on the electrode surface charge distribution.[27-30] In this work the use of CPE instead of pure capacitance has been shown to produce a better fitting. Other research groups have also demonstrated a fitting improving of impedance data for different coated steel systems using CPE.[31] The reason is that the real surface area exposed to the solution is greater than the geometric one, and the degree of surface roughness also increases with exposure time due to the attack to the substrate and coating by the electrolyte. Therefore, it is often better to work with real surface areas which can be several times greater than the geometric one.[2,32] The roughness of a surface is not only a result of the prior grinding and subsequent corrosion, but also due to the presence of dislocations, grain boundaries, and impurities.[33] Also, in the present study, the substrate was grit blasted using Al_2O_3 to reach a mean roughness around 5 μm and the mean roughness of as-sprayed coating surface is around 3 μm. Therefore, for the first sub-circuit $[R_1CPE_1]$ R_1 represents the coating resistance and CPE_1 was associated with the capacitance of the coating, while R_2 and CPE_2 were attributed to the polarization resistance of steel oxidation and capacitance of the substrate/solution interface.

EIS results show no significant benefit for the corrosion resistance of the C20 coating after the heat-treatment at 450°C for 1 h.

Figure 10 shows impedance spectra for 760HT sample recorded at different immersion times as indicated in Fig. 8a. The Nyquist plots for 760HT sample (Fig. 10a1 and a2, where Fig. 10a2 represents a zoom for EIS recorded for more than 1 day of immersion) show very high total impedance for the first day and a strong decrease from the second and following days of immersion. The high total impedance measured for the first day of immersion should be related to the thin and defective passive layer of chromium and nickel oxide formed at the electrode surface as a consequence of the heat-treatment in air atmosphere. For longer immersion times similar impedance diagrams to that for 450HT were obtained, and the total impedance values decreased, probably due to partial or totally dissolution of the thin passive layer by the electrolyte. These results clearly indicate that the coating and its surface, and coating/substrate interface degrade as the immersion time increases. Similar information was obtained from log $|Z|$ vs log f plot (Fig. 10b).

It is also observed that for longer immersion times the frequencies at the maximum phase angle and the total impedance are similar to that measured for C20 and 450HT samples, as expected since the influence of the passive layer is not significant any more.

Figure 10c shows Bode phase angle vs log f plot for 760HT sample recorded for different immersion times. For 1 day of immersion, the diagram suggest the presence of three time constants—at high-frequency range (maximum around 250 Hz), the time constant was attributed to an external and thin passive layer enriched in chromium oxide, which was formed during the short time of heat-treatment, and was simulated by a $[RC_1]$ sub-circuit, at lower frequency range (maximum around 100 mHz) which was related with the substrate oxidation and was simulated by $[RCPE_1]$ sub-circuit,

Downloaded on 2014-01-15 to IP 200.145.3.46 address. Redistribution subject to ECS license or copyright; see ecsdl.org/site/terms_use

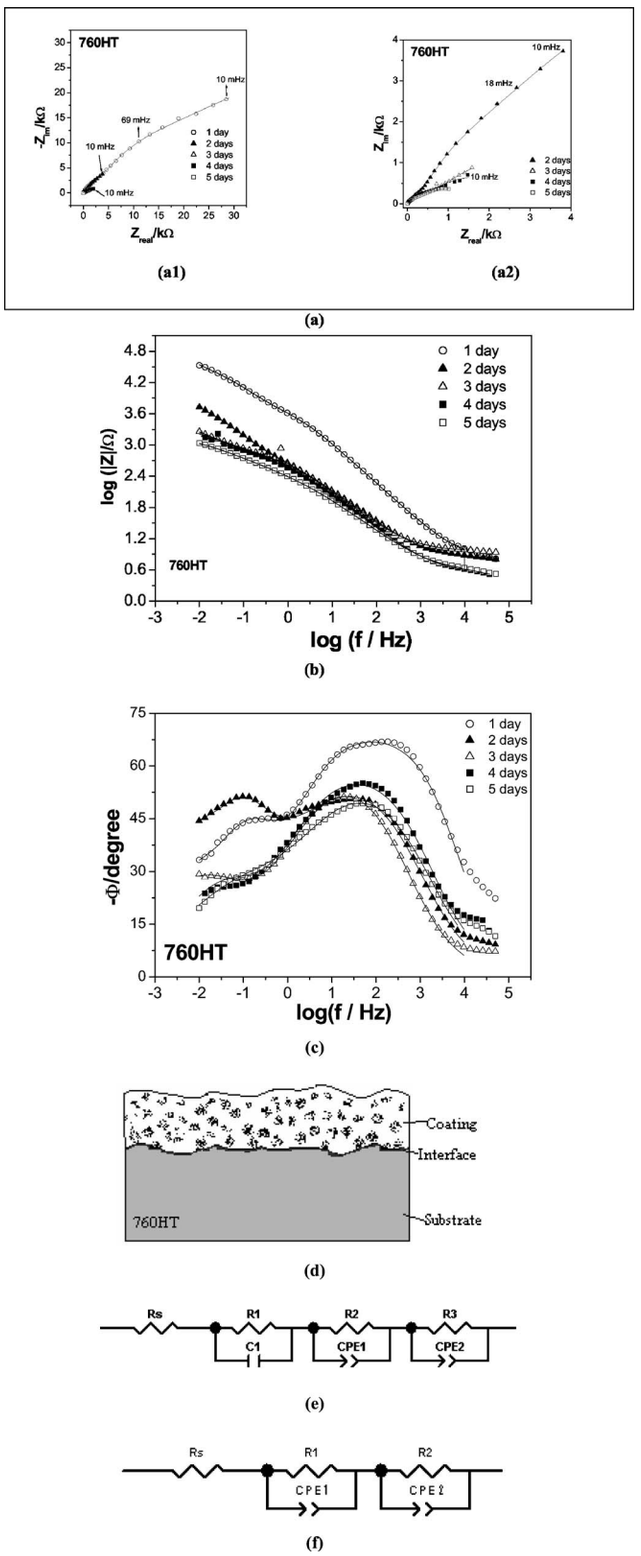

Figure 10. Experimental (symbol) and simulated (solid line): (a) Nyquist, (b) log $|Z|$ and (c) $-\phi$ vs log(f) Bode plots for 760HT -coated steel in aerated and unstirred 3.4% NaCl solution. (d) Scheme proposed for 760HT sample (e) equivalent electrical circuit used for fitting the experimental data for 1 day, of immersion and (f) for longer immersion times. Geometric surface area of working electrode was 0.74 cm^2.

and at intermediary frequencies (maximum around 30 Hz), the time constant not well defined was associated with the Cr_3C_2–NiCr coating. The first and second time constants appeared to be overlapped, and they are placed at the same frequency region of the first time constant for C20 and 450HT samples. For 760HT sample this event was also simulated by a $[R_2CPE_1]$ sub-circuit. The CPE element was here used due to the same reasons mentioned above. Figure 10d shows the scheme proposed for the structure of this sample, which includes a continuous thin surface layer of chromium oxide on the coating surface to the scheme proposed for C20 and 450HT samples. The three time constants were arranged as show in Fig. 10e to give a good fitting of experimental data, in agreement with events occurring in series for short time of immersion (only 1 day).

Bode phase angle plots also show that as immersion time increased the maximum at intermediary frequency is better defined while the one at higher frequency almost disappear. The phase angle (maximum around 50 Hz, in the same frequency range observed for samples C20 and 450HT) decreases from around 70° to values ranging from 45 to 55°, concomitantly, the time constant appearing at lower frequencies was going to a very low phase angle. This means that a continuous coating and substrate degrading is taking place, and that after 1 day of immersion the 760HT sample behaves similar to C20 and 450HT ones. Then, at longer immersion times no significant change in the total resistance of the sample was observed (Fig. 10a and b), which means that the influence of the thin chromium oxide layer can be considered negligible. Therefore, the equivalent circuit shown in Fig. 9d simulates the experimental data (Fig. 10f), where the first $[R_1CPE_1]$ sub-circuit was related to the resistance and capacitance of the coating and $[R_2CPE_2]$ was attributed to the substrate oxidation and capacitance of the coating/substrate interface, the same meaning as defined for C20 and 450HT samples.

Figure 11 shows Bode-phase angle for 880HT series for short and long immersion times together with the scheme proposed for the structure of these samples. For all plots three time constants can be observed—one at high frequencies (maximum around 3 kHz independent of the immersion time) which was attributed to the chromium oxide passive layer and the phase angle increased with the heat-treatment time, one at intermediate frequencies (around and lower 0.2 Hz which shifts to high frequencies with immersion time) attributed basically to the coating itself, and a third time constant (maximum around 0.03 Hz which also shifts to higher frequencies with immersion time) associated with the substrate oxidation. When comparing with 760HT sample it is clear the influence of chromium oxide passive layer present on 880HT series independent of the immersion and heat-treatment times. The increase of phase angle of the highest time constant with the heat-treatment time reveals an increase in the passive character of the sample, probably due to an increase of the chromium oxide layer.

Figure 12 shows impedance spectra for 880HT series recorded at different immersion times as indicated in Fig. 8b-d. Figure 12a1 shows the Nyquist plots for 880HT sample for different immersion times. The total impedance increases from 9 to 121 h of immersion, and then decreases for longer immersion times. For 880HT12 sample EIS diagrams were recorded only up to 110 h (Fig. 12b1) and the behavior is similar to other samples treated at 880°C, but with slightly higher total impedance values. For 880HT24 the total impedance increased from the first up to third day, and then decreased until the end of experiment (around 14 days) (Fig. 12c1). The total impedance values are slightly higher for 880HT12 compared with both other samples treated at 880°C. For 1 h of heating probably the chromium oxide layer is thin and offers lower barrier effect against the electrolyte penetration while for 24 h of heating the strong oxidation produces a thicker passive layer but increases pores and defects all over the sample, mainly at the surface where a great amount of chromium oxides are formed. Similar information can be derived from Bode—log$|Z|$ plots (Fig. 12a2, b2, and c2). Note that even after more than 10 days of test the impedance values are of the same order of magnitude or higher that the values mea-

Downloaded on 2014-01-15 to IP 200.145.3.46 address. Redistribution subject to ECS license or copyright; see ecsdl.org/site/terms_use

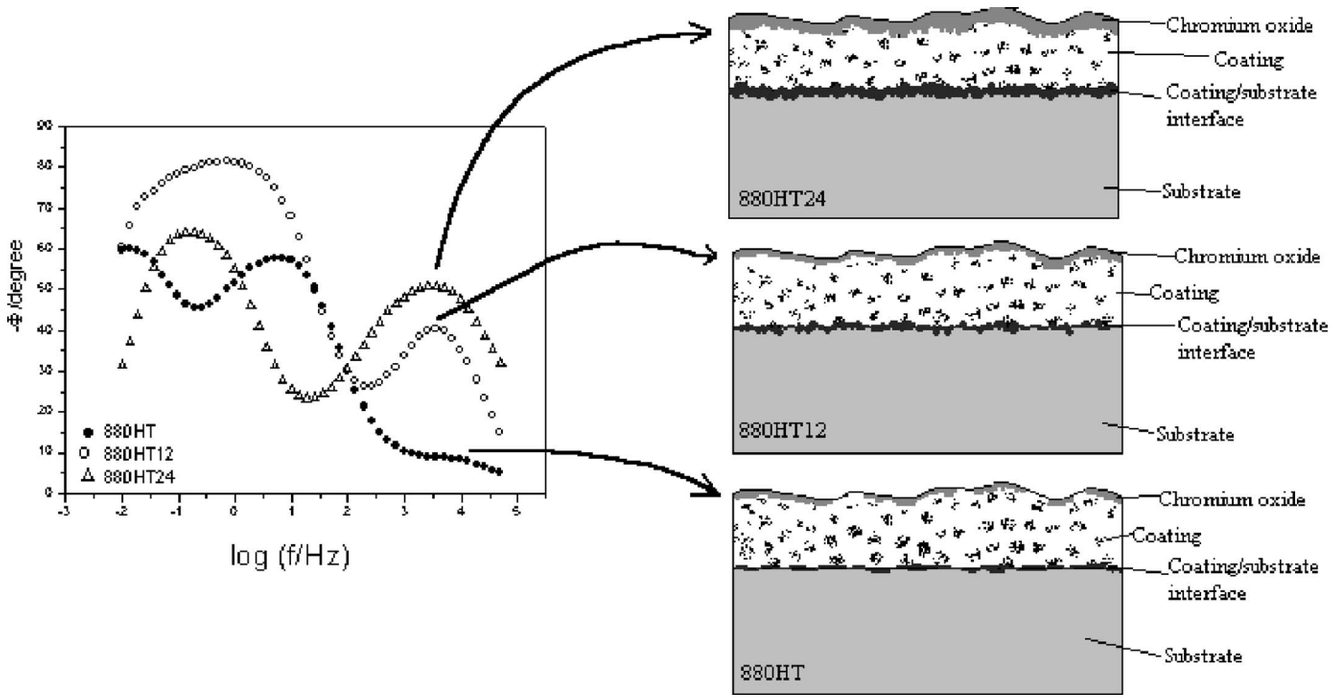

Figure 11. Experimental $-\phi$ vs log(f) Bode plots and corresponding scheme proposed for 880HT, 880HT12, and 880HT24 samples.

sured for 760HT sample after the first day of immersion, demonstrating the positive effect of the heat-treatment at 880°C for protecting the substrate against corrosion in the chloride medium. Among the 880HT series the sample treated for 12 h showed the highest total impedance, almost one order of magnitude greater than the others. More details for this series and the interpretation of EIS diagrams are described for sample treated for 24 h.

The XRD analysis for as-sprayed and grit blasted 880HT24 sample (after removing a layer of around 50 μm thick) (Fig. 3), clearly show that the chromium oxide layer was mainly formed at the outer part of the coating, since its content significantly diminished after removal of some layers. Therefore, the time constant observed at higher frequency range was attributed to the chromium oxide-enriched layer. Therefore, the high resistance associated with the coating was attributed to the presence of this layer, which is also responsible for the shifting of the other maxima to lower frequency ranges when compared to the first time constant for C20 and 450HT and the corresponding one for 760HT samples. The second time constant appeared at intermediary frequency range, the frequency of maximum shifts from around 0.2 to 0.7 Hz and the phase angle continuously diminished from around 65 to 35° as the immersion time increased. These results suggest certain coating degradation with the immersion time. This time constant was mainly associated with the part of the coating between the chromium oxide-enriched layer and the coating/substrate interface. The region includes a certain amount of coating oxidation, defects, carbides decomposition and carbides dissolution and re-precipitation into the supersaturated matrix (see characterization section), which can lead to some pores closing and matrix accommodation delaying the electrolyte penetration. A $[R_2CPE_2]$ sub-circuit was used to simulate the impedance data at this intermediary frequency range. The third time constant was better identified for sample 880HT24 in Fig. 12c3 and c4. In Fig. 12c4 the frequency range was limited to show only events appearing at lower frequency range corresponding to the second and third time constants. Increasing the immersion time the corresponding phase angle rapidly diminished and the resistance decreased (Fig. 12c2) indicating the coating/substrate interface deterioration. This time constant appears at the same region of the second one for C20 and 450HT and for 760HT samples at longer immersion times. It was related to the substrate oxidation and was simulated by an $[R_3CPE_3]$ sub-circuit where R_3 is related with polarization resistance of substrate oxidation and CPE_3 to the capacitance of the coating-substrate/solution interface. The meaning of elements was the same defined before.

The outer passive chromium oxide layer, some oxidation along of the coating and changes produced in the metallic matrix due to carbides decomposition occurred during the heat-treatment, delaying the electrolyte penetration and increasing the corrosion resistance of the system. Among these factors the formation of a chromium oxide-enriched passive layer was the main responsible for the high total impedance measured. Only after a long immersion time (around 225 h), iron oxides were observed on the top of 880HT sample. The iron oxidation and dissolution by the electrolyte reaching the substrate can increase the local iron ions concentration, which move through the coating defects up to the coating surface. If some iron oxide layer is present at the coating/substrate interface it can be dissolved by chloride ions when the electrolyte reaches this region. The coating/substrate degradation leads to a decrease in the phase angle and resistance at lower frequency range.

The impedance results clearly indicate the benefit produced by the heat-treatment applied to the coating for a certain time, which led to an increase of the corrosion resistance as already observed with some mechanical properties for the same kind of coating.[17,18] The 880HT series and mainly the one treated for 12 h showed higher corrosion resistance in chloride solution compared to the different coatings studied, which was mainly attributed to the chromium oxide-enriched layer formed at the outer part of the coating, and diffusion of metallic components to the coating/substrate interface.

Polarizations curves.— Polarization curves recorded using an unstirred and aerated chloride solution after 24 h of immersion are shown in Fig. 13. At this condition, the corrosion potential values were −0.23, −0.24, −0.27, −0.30, and −0.57 V for 880HT24, 880HT12, 880HT, 760HT and 450HT samples, respectively, and the corresponding corrosion current were around 0.4, 0.1, 0.5, 2.1, and

Downloaded on 2014-01-15 to IP 200.145.3.46 address. Redistribution subject to ECS license or copyright; see ecsdl.org/site/terms_use

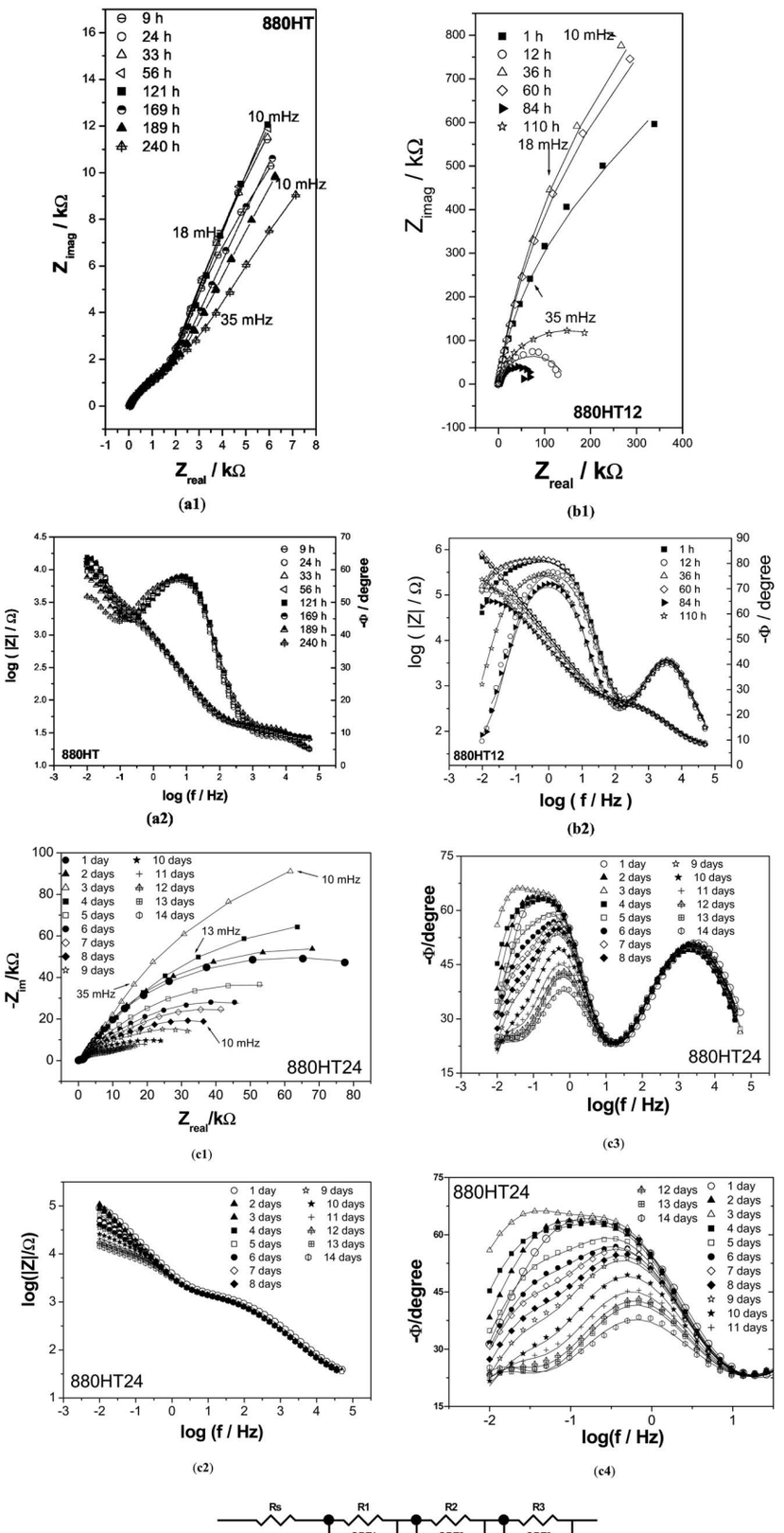

Figure 12. Experimental (symbol) and simulated (solid line): (a1, b1) Nyquist, (a2, b2) log $|Z|$ and $-\phi$ vs log f Bode plots for 880HT and 880HT12 samples. Experimental (symbol) and simulated (solid line): (c1) Nyquist, (c2) log $|Z|$ vs log f and (c3) $-\phi$ vs log f Bode plots, (c4) as in (c3) for a lower frequency range for 880HT24. EIS data obtained in aerated and unstirred 3.4% NaCl solution. (c5) Equivalent electrical circuit used for fitting the experimental data. Geometric surface area of working electrode was 0.74 cm^2.

13.5 μA cm^2 based on the geometric area exposed to the solution. Among the coated steels, the 880HT series showed higher E_{corr} and lower anodic current density values. Among 880HT series the sample treated for 12 h showed lower corrosion current, indicating a higher corrosion resistance, as already demonstrated by EIS experiments. The 760HT sample showed an intermediary behavior be-

Downloaded on 2014-01-15 to IP 200.145.3.46 address. Redistribution subject to ECS license or copyright; see ecsdl.org/site/terms_use

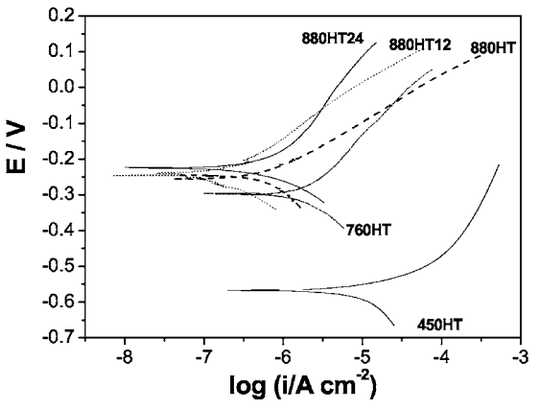

Figure 13. Polarization curves for 450HT, 760HT, 880HT, 880HT12, and 880HT24 samples in aerated and unstirred 3.4% NaCl solution, at 25°C, and $v = 0.166$ mV s^{-1} after 24 h of immersion. Geometric surface area of working electrode was 0.74 cm^2.

tween 880HT sample and 450HT sample. C20 and 450HT samples showed similar polarizations curves and so the curve and data for C20 were omitted. These two samples showed lower corrosion potentials and higher corrosion current density, indicating low quality coatings prepared using standard conditions. These results are in complete agreement with those obtained from OCP and EIS measurements.

After 24 h of immersion in the salt solution, it is likely that the electrolyte penetrated the coating and also attacked in some extension the metallic oxides around the carbides generating easy pathways to reach the substrate. Therefore, the response of a polarization can have great contribution of the substrate mainly for samples C20 and 450HT. Polarization curves were not recorded immediately after the immersion, which certainly should be dominated by the effect of chromium oxide passive layer present at the coating surface.

Conclusions

Chromium carbide-nickel chromium coatings were prepared using HVOF, subjected to a heat-treatment, and characterized with different physical and electrochemical techniques. Physical characterization of the coatings indicated the chromium oxide formation which increases with temperature and heat-treatment time. The heat-treatment at 450°C had no effect on the final properties of the coatings. Heat-treatment at higher temperatures (760 and 880°C) influenced the chromium carbide particles dissolution into the metallic matrix, chromium carbide precipitates formation from supersaturated matrix, and also the chromium oxide amount and distribution, which lead to a different behavior concerning electrochemical results.

The higher amount of chromium oxide formed at the carbide particles and coating surfaces, and Cr and Ni diffusion to the coating/substrate interface contributed to increase the total impedance, corrosion and open-circuit potentials and decrease the corrosion current for samples treated at 880°C. A nickel enrichment of the metallic matrix mainly for 880HT series was also observed. The complexity of the coatings was reflected in a more complex equivalent circuit able to fit electrochemical impedance data.

For C20 and 450HT samples, the influence mentioned above was not observed and the heat-treatment caused no influence on electrochemical results. As a consequence, a simpler equivalent circuit fitted the experimental data.

Acknowledgments

The authors thank the Universitat de Barcelona for the support of the research grant of N.E. They also thank the Ministerio de Ciencia y Tecnología (project no. MAT2003-05004-C02-02), the Generalitat de Catalunya (project no. 2005SGR00310), the FAPESP-Fundação de Amparo à Pesquisa do Estado de São Paulo (project no. 02/00448-7), and CNPq-Conselho Nacional de Desenvolvimento Científico e Tecnológico (project no. 300343/2004-3) for the scholarships.

Instituto de Química da Universidad Estadual Paulista assisted in meeting the publication costs of this article.

References

1. J. M. Guilemany, J. M. Miguel, S. Vizcaíno, C. Lorenzana, J. Delgado, and J. Sánchez, *Surf. Coat. Technol.*, **157**, 207 (2002).
2. A. C. Savarimuthu, I. Megat, H. F. Taber, J. R. Shadley, E. F. Rybicki, W. A. Emery, J. D. Nuse, and D. A. Somerville, in *Proceedings of the International Thermal Spray Conference*, Montreal, Canada (2000).
3. T. Sahraoui, N. E. Fenineche, G. Montavon, and C. Coddet, *J. Mater. Process. Technol.*, **152**, 43 (2004).
4. U. Erning and M. Nestler, in *Proceedings of the United Thermal Spray Conference*, Düsseldorf, Germany (1999).
5. V. Sovolev, J. M. Guilemany, and J. Nutting, *High Velocity Oxy-Fuel Spraying*, p. 397, Maney, London, England (2004).
6. J. M. Miguel, Ph.D. Thesis, University of Barcelona, Barcelona, Spain (2002).
7. P. H. Suegama, C. S. Fugivara, A. V. Benedetti, J. Fernández, J. Delgado, and J. M. Guilemany, *J. Appl. Electrochem.*, **32**, 1287 (2002).
8. J. M. Guilemany, J. Fernández, J. Delgado, A. V. Benedetti, and F. Climent, *Surf. Coat. Technol.*, **153**, 107 (2002).
9. L. Fedrizzi, S. Rossi, R. Cristel, and P. L. Bonora, *Electrochim. Acta*, **49**, 2803 (2004).
10. V. A. de Souza and A. Neville, *Mater. Sci. Eng., A*, **352**, 202 (2003).
11. P. H. Suegama, C. S. Fugivara, A. V. Benedetti, J. Fernández, J. Delgado, and J. M. Guilemany, *Electrochim. Acta*, **49**, 627 (2004).
12. P. H. Suegama, N. Espallargas, J. M. Guilemany, J. Fermández, and A. V. Benedetti, in *Proceedings of the European Corrosion Congress*, Lisbon, Portugal (2005).
13. J. M. Guilemany, J. Fernández, J. Delgadom, and A. V. Benedetti, in *Proceedings of the International Thermal Spray Conference*, Singapore (2001).
14. D. Toma, W. Brandlm, and G. Marginean, *Surf. Coat. Technol.*, **138**, 149 (2001).
15. L. Fedrizzi, S. Rossi, F. Bellei, and F. Deflorian, *Wear*, **253**, 1173 (2002).
16. S. Matthews, M. Hyland, B. James, and T. Levi, in *Proceedings fo the International Thermal Spray Conference*, Orlando, FL (2003).
17. J. He and E. J. Lavernia, *Mater. Sci. Eng., A*, **301**, 69 (2001).
18. S. Matthews, M. Hyland, and B. James, *J. Therm. Spray Technol.*, **13**, 526 (2004).
19. S. Matthews, M. Hyland, and B. James, *Acta Mater.*, **51**, 4267 (2003).
20. L. M. Berger, D. M. Woydt, D. S. Zimmermann, H. Keller, D. G. Schwier, D. R. Enzl, and S. Thiele, Paper presented at the International Thermal Spray Conference ITSC 2004.
21. P. H. Suegama, Ph.D. Thesis, Universidade Estadual Paulista-UNESP, Araraquara, Brazil (2005).
22. J. A. Calero, Ph.D. Thesis, University of Barcelona, Barcelona, Spain (1997).
23. J. N. Clark, D. R. Glasson, S. Amarasiri, and A. Jayaweera, *Thermochim. Acta*, **103**, 193 (1986).
24. A. P. Cheilyarkh and E. G. Fomina, *Russ. Metall.*, **6**, 90 (1999).
25. D. J. Young and B. Gleeson, *Corros. Sci.*, **44**, 345 (2002).
26. S. Armada, Ph.D. Thesis, University of Barcelona, Barcelona, Spain (2001).
27. M. Cai and S. M. Park, *J. Electrochem. Soc.*, **143**, 3895 (1996).
28. D. D. McDonald, in *Techniques for Characterization of Electrodes and Electrochemical Processes*, R. Varma and J. R. Selman, Editors, p. 515, John Wiley & Sons, New York (1991).
29. R. de Levie, *J. Electroanal. Chem. Interfacial Electrochem.*, **281**, 1 (1990).
30. R. de Levie, in *Advances in Electrochemistry and Electrochemical Engineering*, P. Delahay and W. Tobias, Editors, p. 329, Wiley-Interscience, New York (1967).
31. P. L. Bonora, F. Deflorian, and L. Fedrizzi, *Electrochim. Acta*, **41**, 1073 (1996).
32. P. L. Ko and M. F. Robertson, *Wear*, **252**, 880 (2002).
33. C. Liu, Q. Bi, A. Leyland, and A. Matthews, *Corros. Sci.*, **45**, 1243 (2003).

Downloaded on 2014-01-15 to IP 200.145.3.46 address. Redistribution subject to ECS license or copyright; see ecsdl.org/site/terms_use